

Dual-sided transparent display enabled by polymer stabilized liquid crystals for augmented reality

Received: 19 April 2024

Accepted: 30 October 2024

Published online: 11 November 2024

 Check for updates

Suman Halder¹, Yunho Shin², Yidan Peng³, Long Wang³, Liye Duan³, Paul D. Schmalenberg⁴, Guangkui Qin³, Yuxi Gao³, Ercan M. Dede⁴, Deng-Ke Yang^{1,2} & Sean P. Rodrigues⁴ 

In the past decade, display technology has been reimagined to meet the needs of the virtual world. By mapping information onto a scene through a transparent display, users can simultaneously visualize both the real world and layers of virtual elements. However, advances in augmented reality technology have primarily focused on wearable gear or personal devices. Here we present a single display capable of delivering visual information to observers positioned on either side of the transparent device. This dual-sided display system employs a polymer stabilized liquid crystal waveguide technology to achieve a transparency window of 65% while offering active-matrix control. An early-stage prototype exhibits full-color information via time-sequential processing of a red-green-blue light-emitting diode strip. The dual-sided display provides a perspective on transparent mediums as display devices for human-centric and service-related experiences that can support both enhanced bi-directional user interactions and new media platforms.

Augmented reality (AR) is fusing the realm of sensors and user interfaces, in a way that allows a person to interact more seamlessly with their environment or other people. This interplay of online interactions within our immediate environment, brought about by AR, has forced the display industry to rethink the methods through which displays are created. The momentum in this space is enabling rapid transformation of display systems to meet the growing demands of AR, specifically by creating displays that integrate digital imagery from a user's perspective. Typically, AR devices are commercialized as wearable technology, which offers personalized information to augment the user's view.^{1–10} In a similar fashion, although not typically regarded as tools for AR, transparent display panels serve a dual purpose offering both a window to visualize a scene while simultaneously displaying overlaid information.^{11–13} To bridge this gap between transparent displays and augmented reality devices and to recognize transparent displays full potential as AR tools, a series of challenges remain. The first nontrivial problem is the tradeoff that exists between

brightness and transparency. Current commercial transparent displays only provide transparency ranging from 33–45% for organic light-emitting diode (OLED) technologies such as LG's 55EW5PG-S at 38% at 400 nit and OLED Space at 45% and 200 nit,^{14–17} 10–20% for polarized liquid crystal display (LCD) panels^{18,19}, 70–90% for photoluminescent displays²⁰, and 85% light plate/waveguide devices.²¹ Commercial OLED and LCD technologies demonstrate brighter screens, while light plate devices have yet to maximize their scattering efficiencies^{18,22} and photoluminescent screens lack multi-color integration on a pixel level. In addition to these specifications, there remains a secondary challenge with transparent displays, known as “bleed-through,” that prevents broader market realization.^{23,24} Bleed-through occurs when a display shows an image on the front, while a mirrored version of that image becomes visible on the rear side of the display. For this reason, the application of a single-image transparent display is limited to areas where only the front side can typically be observed, for instance, in a residential or commercial setting like a shopping window that is

¹Department of Physics, Kent State University, Kent, OH, USA. ²Advanced Materials and Liquid Crystal Institute, Kent State University, Kent, OH, USA. ³Central Research Institute, BOE Technology Group Co., Ltd., Beijing, China. ⁴Electronics Research Department, Toyota Research Institute of North America, Ann Arbor, MI, USA. ✉ e-mail: Sean.rodrigues@toyota.com

furnished with a backdrop. Furthermore, the absence of user privacy poses a significant hindrance, preventing the commercialization of bleed-through transparent displays in both corporate settings and personal smartphone use.^{11,25–30} In order to expand the application of these displays to environments where people may be present on both sides, i.e., most vehicle and building windows, this bleed-through issue must be addressed to realize effective transparent display systems. While transparent, AR displays may be functional in one direction, their purpose and value depreciate when the device cannot be made dual-sided. While this paper does not delve into a comprehensive review of transparent display technologies, readers can discover valuable insights on transparent LCDs, transparent OLEDs, projection technologies, and noteworthy highlights from commercial ventures, which are most effectively summarized in reviews from events such as the Consumer Electronics Show (CES) and the Society for Information Display, Display Week.

As proposed in this paper, dual-sided transparent displays, visualized in Fig. 1, provide an augmented surface enabling information sharing to two viewers simultaneously while maintaining a transparent window between each viewer. Dual-sided transparent displays could amplify interactions and remove some of the unique discomfort that comes from wearable augmented reality technology. As an example, a dual-sided display, owned by a third party can be used between two users without concern for one of the two users recording personal interactions. Specifically, we expect dual-sided display technology to enhance customer-facing interactions such as ridesharing interfaces, checkout lines at grab-and-go food locations, work productivity, and next-level gaming. The use-case of the dual-sided display as an augmented reality device is further elucidated in Fig. 1a as a ride-share experience where the single pane display provides two perspectives. Fig. 1b shows the window from the perspective of an English-speaking driver who is notified that the passenger is being confirmed as the correct individual. Meanwhile, a Japanese-speaking tourist is requested to enter their driver code on a screen that presents a dial-pad to them on the exterior of the vehicle

(the rider code would be pre-emptively shared with them on their phone), as shown in Fig. 1c.

To produce such a device, there are three immediate challenges, illustrated in Fig. 1d–f, that we describe as the 3-O's, occlusion, obstruction, and obversion. The first O is occlusion, which describes how one object hides another behind itself.^{31,32} With regards to the display, the device cannot allow information shown on one side to obscure information that is shown on the other. Therefore, stacking two layers of transparent OLED panels would not suffice to create a dual-sided display. The second O is obstruction. This implies that the device should operate as a window when not in use, and an interlayer material between the displays would block the view and is not desired. Finally, the third O is for obversion, which stands in place for the description of bleed-through as described earlier. Obversion of an image, presented on an initial side, should be prevented from being shown on the opposite of the display in the form of a mirrored image, thus providing potentially unintelligible information to an unintended viewer. If the challenges proposed by these three O's can be overcome, an effective augmented reality device can be assimilated into any window-based viewing system.

Computer science and human-machine interface research groups have investigated human interactions and experiences utilizing dual-sided displays by projecting information onto half mirrors or tinted windows at specific angles to minimize light transmission.^{24,28} Another group utilized liquid crystal display and polarizing components to achieve their goals.²⁸ These existing demonstrations provide unique solutions utilizing off-the-shelf components to create their displays, thereby limiting the fundamental advancement of the device specifications. To create a high-performance commercial device, the base technology should be modified to achieve a strong brightness, high transparency, and sharp contrast ratio device. As a launching point, for the work presented herein, we recognize the efforts of a “single” sided, transparent display created from an edgelit light plate, where the liquid crystal panel acts as the conductor for the light and ITO electrodes are utilized to activate the pixels from their off to on-state.^{33–36}

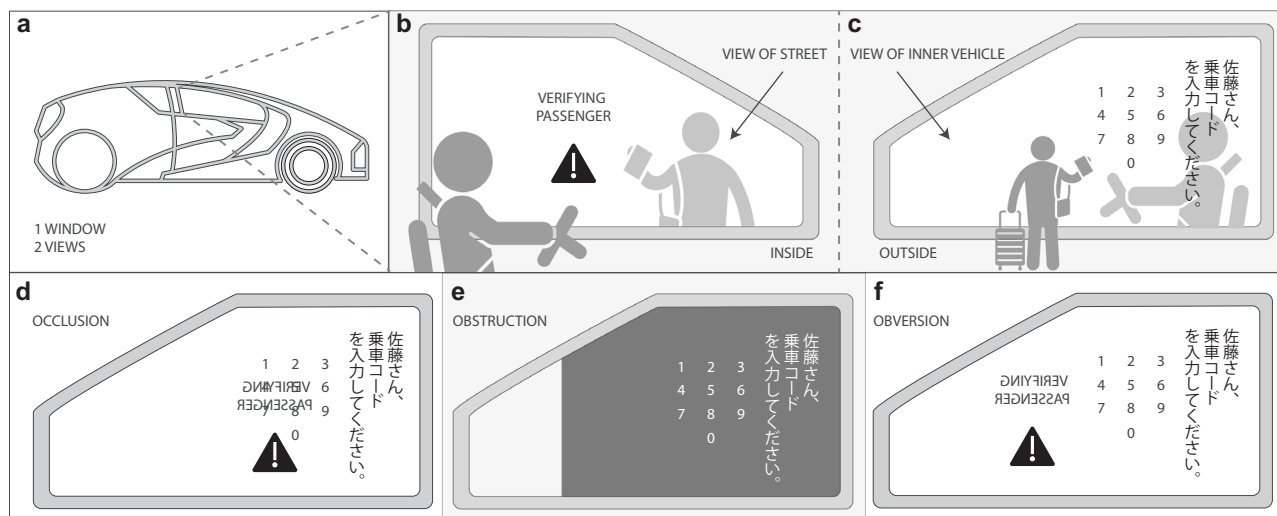


Fig. 1 | Concept for a dual-sided transparent display. **a** A vehicle installed with a dual-sided display could utilize one window to provide two unique augmented scenes. Here an interaction between two people, one English-speaking and one Japanese-speaking, is enhanced using the dual-sided display in the case of a ride-share application. **b** A depiction of what the English-speaking driver would see from the inside of the vehicle is shown on the interior side of the window. Note that the majority of the screen remains transparent allowing the driver to see the passenger. **c** A depiction of what the Japanese-speaking passenger would see approaching the vehicle; the Japanese translates to “Sato-san, please enter the boarding code.” Note that although the same window is used, graphics are shown on either side without

any impact on each other **d–f** Most technologies related to the application of a dual-sided display suffer from the following three challenges. **d** Occlusion implies that graphics on one side of the display block those on the other side; in this case, the desired writing occludes the obverted writing. This overlap of text and or graphics detracts from the utility of the display. **e** Although an interlayer could be used between two screens, this type of occlusion removes functionality as an augmented reality device. **f** By using software it is possible to defeat the challenge of occlusion using a single screen by separating out the images, however, the obverted imagery would not be desired by a user.

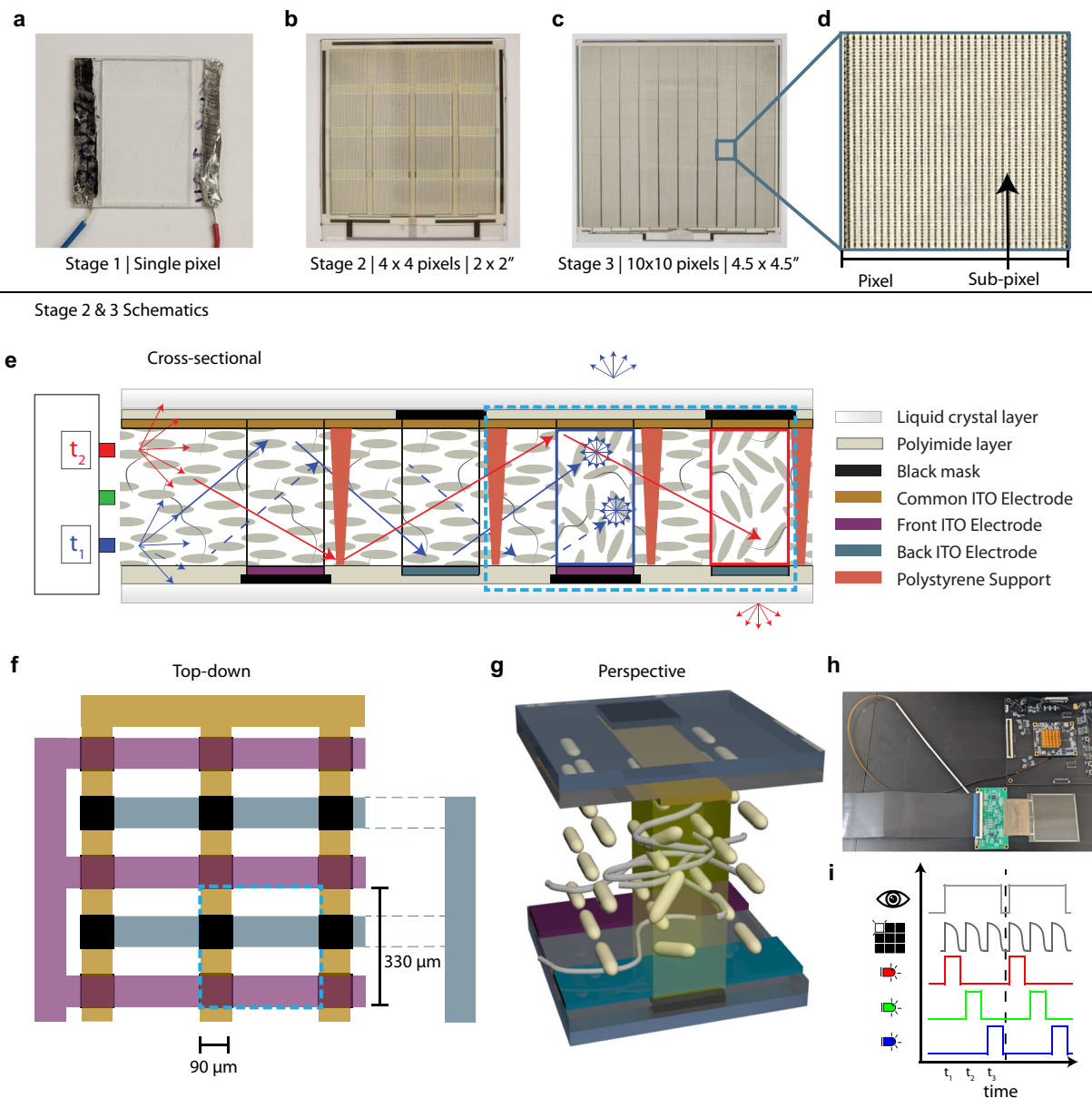


Fig. 2 | Design and operation of the dual-sided transparent display. **a** The Stage 1 prototype is a single-pixel device that allowed for early-stage testing of the liquid crystal cell. **b** The Stage 2 prototype has 16 total macro-pixels that can be controlled independently. **c** The Stage 3 device is composed of 100 individual macro-pixels. Control wiring connects to the lower portion of each device. **d** Zoom in of a single pixel. Each pixel is composed of a set of 33×33 unit cells. **e** A cross-sectional schematic of the dual-sided display, with 2 sample time frames for the time-sequential processing, t_1 & t_2 . The dashed line represents a single-pixel, unit cell

that is composed of 2 sub-pixels, one that faces the driver and one that faces the passenger as schematically described in Fig. 1. Scattering is blocked to the undesired side by a black mask. **f** A top-down schematic of the electrodes for Stage 2 and Stage 3 devices, where the labels for the electrodes are shown in (e). **g** A perspective schematic that depicts the liquid crystal and polymer network. Here a single sub-pixel, highlighted in yellow, is scattered within a pixel, unit cell. **h** A top-down image of the dual-sided display, its driver, and its LED. **i** A pictorial description of time-sequential color graphics.

In this paper, we demonstrate an early prototype of a dual-sided transparent display utilizing liquid crystal technology through a light plate. The device demonstrates imagery on both sides of the display without any crosstalk and does not suffer from occlusion, obstruction, or obversion. Moreover, the device retains a transparency of 65% and an average brightness of 16 cd/m^2 .

Results

Design

Three research stages of display cells were utilized in the development of the dual-sided transparent display. Each stage is slightly different but maintains three functional components, an LED light source that shuttles light through the light plate display, the liquid crystal that

scatters the light, and the electrodes that control the liquid crystal modulation. The three stages of the display shown in Fig. 2 were implemented in order to reduce complexity and cost throughout the material research design phase.

The Stage 1 display, shown in Fig. 2a, is the easiest and cheapest display to fabricate, thereby allowing early-stage parametric testing of the polymer-stabilized liquid crystal matrix. The Stage 1 device is a single-pixel, waveguide display that portrays identical images on either side of the display. It should be noted that the Stage 1 display is not the proposed dual-sided display as it creates mirrored images on both sides of the display, rather than two unique non-interfering images. This prototype device consists of indium tin oxide (ITO) patterned on two glass substrates, separated by micron-sized spacers, and filled with

a liquid crystal matrix. The ITO is patterned into electrodes that are 25 μm in width (active area) and a non-ITO strip of 250 μm (inactive/transparent area); a schematic of the device can be found in Supplementary Fig. S1. Next, an alignment layer of polyamide (PI) SE2171 from Nissan Chemical is coated on the ITO and then rubbed to create homogeneous alignment. The cell is created by joining both patterned pieces of glass and creating a cell gap that is uniformly controlled at 2 μm using spherical spacers. The cell gap of 2 μm was chosen after evaluation of the cell performance when utilizing 2, 3, and 4 μm spacers see Supplementary Fig. S2. The cells were filled with a mixture of a monomer, the nematic liquid crystal BOE-5, and a photoinitiator Benzoin methyl ether (BME). After the mixture is injected into the display cell, the cell is irradiated by ultraviolet (UV) light, and the monomers are polymerized to form a polymer network within the liquid crystal matrix.

In addition to the Stage 1 single-pixel device, Stage 2 and Stage 3 devices are developed that enable unique non-interfering images to be portrayed on either side of the display. The Stage 2 prototype, as shown in Fig. 2b, is a 2" \times 2" display that consists of 16 individually controllable macro-pixels in a 4 \times 4 matrix. The Stage 3 display, as shown in Fig. 2c, is a 4.5" \times 4.5" display that consists of 100 individually controllable macro-pixels in a 10 \times 10 matrix with the same resolution per pixel as the Stage 2 display. Each single macro-pixel contains 31 \times 31 sub-pixels that aim out the front of the display and another set of the same amount that aims out the rear of the display; refer to Fig. 2d. While Stage 2 and Stage 3 prototype devices have resolutions of only 16 and 100 individually controllable macro-pixels, respectively, these designs were carefully selected to balance cost when prototyping the devices; in the future, each sub-pixel (shown in Fig. 2d) can be independently controlled utilizing a specialized electronic control unit. To protect from bleed-through and therefore the obversion obstacle, both Stage 2 and Stage 3 displays involve a more complicated panel, layer stack up.

A cross-section of both Stage 2 and Stage 3 devices is shown in Fig. 2e. The displays operate by injecting light from an LED array on the left side of the diagram into the waveguide. Within the waveguide, a polymer-stabilized liquid crystal is present, which either allows the light to pass through in the off-state or scatters light perpendicularly out of the display in the on-state due to the oscillating reorientation of the liquid crystal. The function of the polymer network is to create a polydomain liquid crystal structure which enables this scattering when the voltage is applied and utilizes elasticity to quickly relax the device to its off-state. An interleaved matrix of ITO electrodes is arrayed, as shown in the top-down view in Fig. 2f, to control the on/off-state of individual pixels in the display matrix when a voltage bias is applied. Common ground ITO electrodes are distributed on the top side of the display, and two sets of activation electrodes, one for creating an image on the front of the display, and the other for the back, are interdigitated on the bottom side of the panel. An individual single pixel is shown in a perspective view in Fig. 2g and is denoted as a dashed line in Fig. 2e, f. Since this is a multipixel active-matrix display, each of the single-pixel, unit cells are divided into three parts: a sub-pixel with one active region for the inside viewer, a sub-pixel with one active region for the outside viewer, and an inactive region to function as a transparency window. In each single-pixel, unit cell, a black mask is applied to one sub-pixel on one side of the waveguide to block light from escaping; this mask is key to providing light to only the desired side and preventing light from leaking to an unintended viewer. The size of the black mask is designed to be large enough to block all the light from a dedicated sub-pixel but small enough to maintain sufficient transparency of the entire panel. The dimensions of the black mask that cover one sub-pixel are 100 μm \times 100 μm and the dimensions of the active area of the sub-pixel are 90 μm \times 90 μm . Molybdenum/Aluminum/Molybdenum (Mo/Al/Mo) wiring is utilized to connect to terminals at the edges of the ITO strips, where Mo serves as an adhesive layer.^{37,38} The same methods that are utilized for the liquid crystal,

that is applied to Stage 1 devices, are also used in filling the Stage 2 and 3 systems. The cell thickness of this manufactured device with an active matrix is limited to a 3 μm thickness due to processing conditions and is controlled by styrene posts. Although the preferred thickness of 2 μm was demonstrated in our Stage 1 device, fabrication feasibility for these prototypes was limited to 3 μm for the Stage 2 and 3 devices. Similarly, the operation of the device is achieved by injecting light via an LED into the sides of the display, and a 1 kHz voltage is applied across the electrodes, which rotates the liquid crystals and induces scattering in the display.

Characterization

In the development of the display, we structured parametric studies of the Stage 1 devices, Fig. 2a, to investigate key factors that impact the performance of the display, while utilizing a low-cost research prototype. The results from these parametric studies are provided as plots of applied voltage versus light intensity scattered from the display in Fig. 3a–c, while Fig. 3d–f provide bar chart analyses of these studies in the form of contrast ratio and saturation voltage. The contrast ratio (CR) is a crucial parameter of image quality for a liquid crystal display, especially a waveguide display, which is defined as the ratio between on- and off-state light intensities, $CR = I_{\text{max}}/I_{\text{min}}$. Therefore, low light leakage at the off-state and high light intensity at the on-state is desirable for sharp contrast and enhanced brightness of a display. The second parameter, the saturation voltage V_{sat} , is defined as $V_{\text{sat}} = V(I_{\text{min}}) + 0.9[V(I_{\text{max}}) - V(I_{\text{min}})]$ and in this paper it refers to the voltage level required to fully activate (or saturate) the liquid crystals in a pixel, where $V(I)$ is the function described by the voltage vs. intensity curve, I_{max} is the maximum intensity of light scattering, and I_{min} is the minimum intensity of light scattering on the curve like those shown in Fig. 3a–c. In addition to the CR, the saturation voltage is a key determinant in selecting which configuration moves to the next device stage. In our case, we prefer a lower voltage for the saturation voltage as this implies a lower operating power.

Polymer-stabilized liquid crystals utilize, the polymerization of various monomers to impact the resting state, scattering coefficient, and switching speed of the liquid crystal. As an initial study, we investigate the influence of the monomers on the electro-optical properties of the display in the Stage 1 device. Each of these monomers are proprietary blends. The variation in electro-optical properties of the polymer-stabilized liquid crystal once crosslinked with monomers HCM-009, BAB-6, RM-82, and RM-257 can be primarily attributed to the structural differences in the monomers' mesogenic bifunctional diacrylate configurations. The electro-optical performance is influenced by the length of the rigid core and the flexible tail of these mesogenic monomers. More details are provided in the supplementary information. The applied voltage-dependent light intensity curve of the displays with various monomers combinations are shown in Fig. 3a, b. Upon analysis of the graph in Fig. 3a, it is evident that the Stage 1 device fabricated with monomer HCM-009 exhibits notable light scattering capabilities with a maximum light intensity (I_{max}) slightly exceeding 5 a.u., accompanied by an off-state intensity (I_{min}) of approximately 0.22 a.u. Furthermore, this configuration exhibits maximum brightness when the display is in the on-state and reduced light leakage from the display in the off-state, resulting in a contrast ratio of approximately 24, thus establishing HCM-009's superiority over the other monomers investigated herein. The saturation voltage associated with HCM-009 measures 10.5 V. The next best monomer is RM-257. The electro-optical performance of monomer RM-257 is moderate, with a maximum light intensity, $I_{\text{max}} = 4.1$ a.u., an off-state intensity of $I_{\text{min}} = 0.26$ a.u., a $CR = 15.9$, and $V_{\text{sat}} = 12$ V. Though the saturation voltages of the displays prepared using monomer BAB-6 and RM-82 are low, ~9 V, other electro-optical properties such as the on/off-state light intensity and contrast ratio are less satisfactory. Based on these results, we selected HCM-009 for further prototypes.

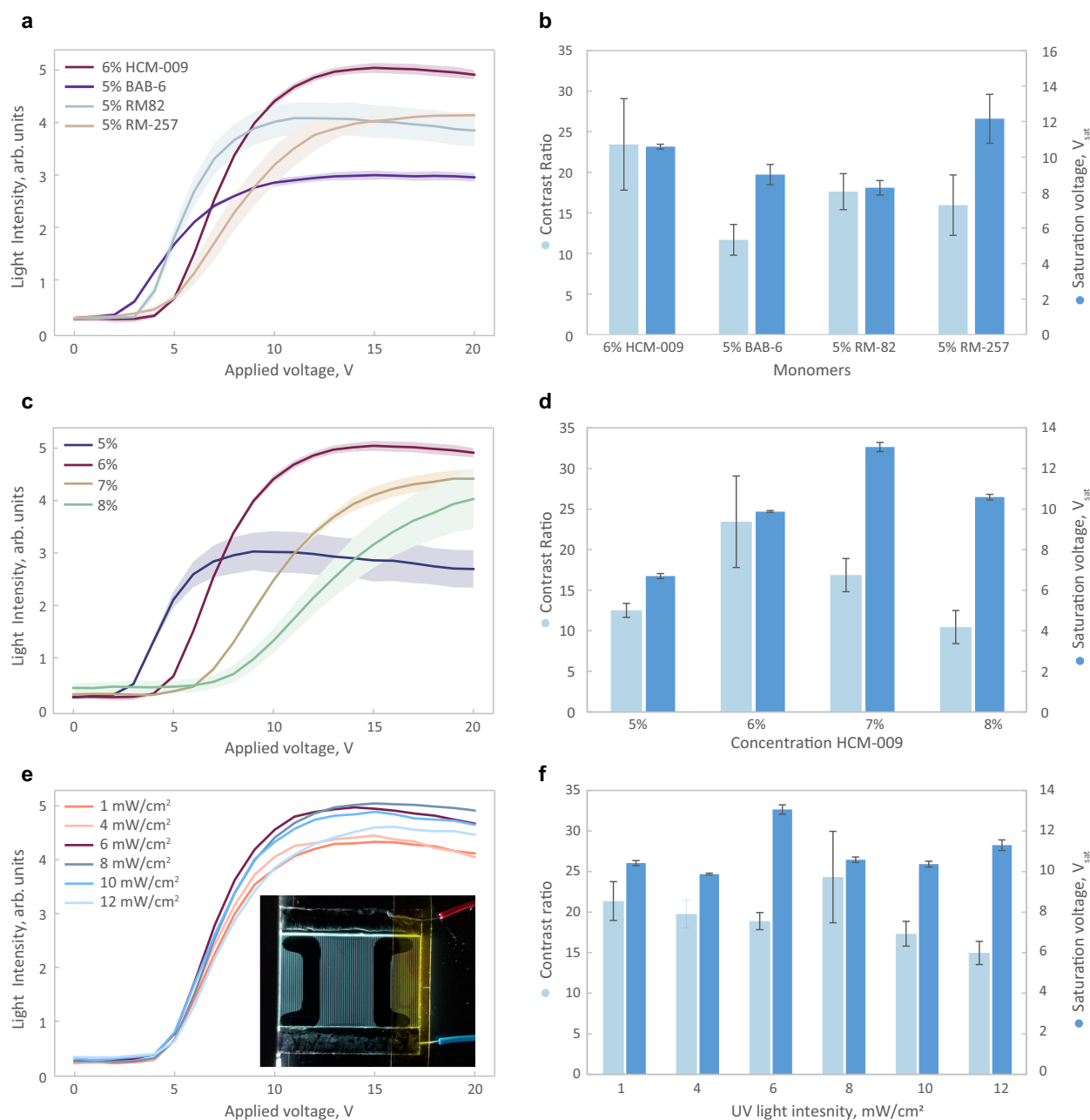


Fig. 3 | Optimization of cell conditions in Stage 1 devices. a, c, e Studies of scattered light intensity vs voltage for different conditions in the Stage 1 cell and **b, d, f** their corresponding contrast ratio and saturation voltage. **a, b** A variety of polymerization monomers are evaluated. HCM-009 maintains both a modest

contrast ratio and saturation voltage and is therefore selected to continue with further studies; **c, d** Varied concentrations of HCM-009 are assessed; **e, f** UV polymerization intensities are varied with the HCM-009 monomer.

After studying the electro-optical properties of the different monomers, we optimized the concentration of the best-performing monomer, HCM-009. The applied voltage versus light intensity curve at various HCM-009 concentrations is shown in Fig. 3c and Fig. 3d provides the corresponding CR and saturation voltages. As the monomer concentration increases, the saturation voltage increases until it reaches a maximum at 7%. Meanwhile, the best CR is achieved at a concentration of 6%, thereby maximizing the light intensity relative to the off-state.

With the optimized 6% concentration of HCM-009 selected, a parametric study of the UV light intensity needed for polymerization was performed; the results depicted in Fig. 3e, f, showcase the relationship between light intensity and applied voltage. Notably, both the

off-state light intensity and the maximum light intensity show an increase in UV light intensity up to 8 mW/cm², but then subsequently declined. Thus, the UV polymerization intensity of 8 mW/cm² is optimal. Given these parameters, a contrast ratio of 24 is achieved. Furthermore, it is worth noting that the driving voltage initially decreased from 10.4 V to 9.9 V at an intensity of 6 mW/cm² before undergoing a subsequent increment.

To conclude the studies regarding the Stage 1 device, the switching time or switching speed was measured for a variety of configurations of the devices. In general, the switching speed did not show remarkable improvements from the switching time shown in Fig. S3, which was measured for the 6% HCM-009 device, with a UV curing intensity of 8 mW/cm². The cell turn-on time is 1 ms, and the turn-off

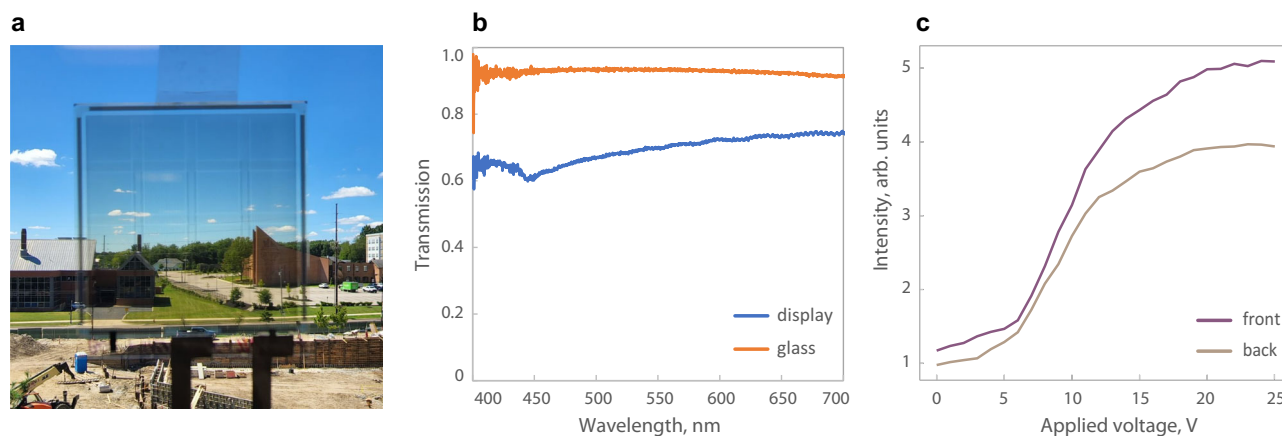


Fig. 4 | Prototype characteristics of the dual-sided, liquid crystal display.

a Image of the Stage 2 display demonstrating the transparency of the device. The wiring for the device would connect at the bottom and the LED strips would fill the display with light from the left and right side. **b** Transmission spectra of the display

are shown relative to a single glass pane. The transparency loss in the display can be attributed to the black mask, the first air-to-glass reflection, and absorption from materials like ITO, among others. **c** Plot of scattered light intensity as a function of voltage is provided for both the front and back of the dual-sided, 4×4 pixel display.

time is ~ 2 ms, which allows for time-sequential operation of the device to generate a full-color image. Full-time sequential operation allows the display to operate without having to rely on color filters embedded into the device, which would decrease the transparency of the display.

After the monomer selection and process optimization in the test cells was complete, the Stage 2 and Stage 3 prototype displays shown in Fig. 2 were fabricated. In Fig. 4a, an image of the Stage 2 prototype against a blue sky at the Kent State campus is demonstrated to show the transparency of the display. In Fig. 4b, a comparison between the transmission spectrum in the visible regime is shown for the display and a single pane of glass for reference. The transparency of the Stage 2 device relative to air is approximately 65% over the visible range, indicating its optical clarity when the device is inactive. The loss of light relative to the pane of glass can be mainly attributed to the presence of the black mask and the ITO electrodes. The ratio of the black mask to the transparent region of the liquid crystal can be calculated as 18% leading to a sizable loss in transparency. The ratio of the black mask to transparent window can be calculated as follows: there are two black masks that define the active sub-pixels that face either side, so we can calculate the ratio as $(2 \times (100 \mu\text{m})^2) / (330 \mu\text{m})^2$ where $100 \mu\text{m}$ is the length of one side of the black mask, and $330 \mu\text{m}$ is the length of one side of the pixel, including both the black mask and transparent region as shown in Fig. 2e or 2g. The voltage-dependent electro-optical properties were also measured for the display. As shown in Fig. 4c, measurements of the scattered light intensity are obtained from the middle of the device, between the two input light sources on either side of the LCD panel. The plots demonstrate a noticeable difference between the front and rear sides of the display in terms of light intensity, with the front side exhibiting a slightly higher overall light intensity.

Based on these measurements, we determined the contrast ratio of the display to be approximately 4.34; as mentioned previously this value indicates the distinction between the brightest and darkest areas of the display. Additionally, we measured the brightness of the display to be approximately 16 cd/m^2 , signifying its luminous intensity. These findings provide valuable insights into the optical performance of the Stage 2 display and its suitability for further evaluation and optimization.

Finally, a Stage 3 display cell was demonstrated and powered by a driver board to display different images utilizing time-sequential processing. The display can be seen in various conditions as shown in Fig. 5 and Supplementary Movie 1. Fig. 5a provides an image of the display with the LED array integrated into a housing. The image is taken indoors under ambient light conditions. The housing supports the flex ribbon and associated board that is attached to the display and also serves to secure the LEDs tight to the side of the waveguide display.

Fig. 5b, c show the front (Side A) and back (Side B) views of the display, respectively. The display images shown on either side do not interfere with each other, therefore, in combination, the images confirm the operation of a true dual-sided transparent display system. Moreover, the images in the dark regions are, in fact, transparent as the images were taken in a dark room. The transparency of these regions can be visualized in Supplementary Movie 1.

Discussion

In this article, we demonstrated a dual-sided transparent display. The display operates by injecting light from LEDs through a light plate into the side of the display, where the light plate scatters the light through the actuation of liquid crystal pixels. Three different stages of the device were prototyped, where the Stage 1 device was used to parametrically optimize the materials utilized for the display, and the Stage 2 and 3 devices enabled small-scale evaluation of active-matrix modulated devices. By parametrically studying the monomer type, monomer concentration, and UV intensity, the conditions for creating an optimum stage 2/3 device were obtained. The parametric studies of the Stage 1 device achieved a contrast ratio of ~ 24 and a driving voltage of about 10.5 V for the single-pixel display. At present, the multipixel display demonstrates a transparency of 65%+ over the visible window, a contrast ratio of approximately 4.34, and a brightness level of 16 cd/m^2 .

A variety of enhancements are possible as a next step. In the current state of the device, the full potential of the resolution of the device is underutilized. Each pixel within the 10×10 pixel device is composed of many smaller sub-pixels that are each $90 \mu\text{m} \times 90 \mu\text{m}$ in size. These smaller sub-pixels could be individually controlled, however, the cost to develop a unique driving board with this resolution would increase the price significantly with little benefit at this stage of the device design. Connecting groups of sub-pixels to form macro-pixels, provided an opportunity to evaluate the brightness and contrast ratio of a high-resolution device while keeping upfront investments low. Individually controlling these sub-pixels is estimated to increase the display resolution by more than 300 times. Second, further optimization of the pixel size and coupling of the LED light into the light plate waveguide is expected to further increase brightness and improve the contrast ratio of the device. Specifically, in the current setup, it was necessary to be able to easily switch the LED from one device to another in a modular fashion for fast prototype evaluation. However, as a result, the total coupling of light into the device from the LED was deemed inefficient based on observed light leakage from the edge of the display during prototype tests. Finally, the relative loss in

contrast ratio from the Stage 1 to Stage 3 prototype can be attributed to the presence of the black mask and the pixel arrangement of the device; see the supplementary information section titled electrode layout. Further optimization of the contrast ratio would likely require

novel liquid crystal mixtures to operate the transparent, active-matrix technology.

To conclude, we envision this dual-sided transparent display technology as having applications in a variety of environments including informative displays such as office and vehicular windows, enhanced customer-facing interactions such as ridesharing interfaces, checkout lines at ice cream, fast food, or translation services, and user-user augmented discussions such as in-office communications, and gaming platforms with similarities to a battleship-like game.

Methods

The Stage 1 display was fabricated using two parallel ITO-coated glass substrates. The top substrate was patterned into striped ITO electrodes (active area) of $25\ \mu\text{m}$ and no ITO regions (inactive area) of $250\ \mu\text{m}$, while the bottom substrate was covered fully by ITO with no pattern. See the Supplementary Information, Fig. S1. The cell gap was uniformly maintained at $2\ \mu\text{m}$ using spacers. In all stage devices 1, 2, and 3, an alignment layer of polyamide (PI) SE2171 was coated on the ITO and then rubbed to create a homogeneous alignment. In stage 1 devices, the cells are filled with a mixture of monomer, nematic liquid crystal BOE-5, and photoinitiator BME, where percentages are dictated by the monomer concentration. The stage 2 and stage 3 cells are filled with a mixture of monomer at 6%, nematic liquid crystal BOE-5 at 93.5%, and photoinitiator BME at 0.5%. The cells are irradiated with a UV lamp in a room temperature environment with a wavelength around $365\ \text{nm}$ at an intensity of $8\ \text{mW}/\text{cm}^2$ for 30 min, allowing the monomers to form a polymer network. The UV polymerization wavelength falls within the absorption range of Benzoin methyl ether, our chosen photoinitiator, which is $220\text{--}370\ \text{nm}$. The liquid crystal BOE-5 is a proprietary liquid crystal specifically designed for active-matrix applications. It has a birefringence (Δn) of 0.25, a dielectric anisotropy ($\Delta\epsilon$) of 36, and a nematic to isotropic transition temperature of $100\ ^\circ\text{C}$.

For the electro-optical properties study, we measured the light scattered in response to an applied AC voltage at a frequency of $1\ \text{kHz}$. We used an RGB LED strip (BOE) as the light source and a photo-detector (OREAL) as the light detector. The signals were processed using a DAQ system (National Instruments, BNC-2090) combined with a function generator (Analogic, Measurimeter-II).

The transparency of the device was measured using a spectrometer. Light from a broadband tungsten-halogen light source was passed through the stage 2 and stage 3 devices in an off-state. The light was then collected by a Horiba IHR320 and detected on a thermoelectrically cooled Synapse CCD.

Data availability

All key data that support the findings of this study are included in the article and its Supplementary Information. Additional datasets and raw measurements are available from the corresponding authors upon request.

References

- Xiong, J., Hsiang, E.-L., He, Z., Zhan, T. & Wu, S.-T. Augmented reality and virtual reality displays: emerging technologies and future perspectives. *Light Sci. Appl.* **10**, 216 (2021).
- Yin, K. et al. Virtual reality and augmented reality displays: advances and future perspectives. *J. Phys. Photonics* **3**, 022010 (2021).
- Yin, K. et al. Advanced liquid crystal devices for augmented reality and virtual reality displays: principles and applications. *Light Sci. Appl.* **11**, 161 (2022).
- Szczerba, J., Hersberger, R. & Mathieu, R. A wearable vibrotactile display for automotive route guidance: evaluating usability, workload, performance and preference. *Proc. Hum. Factors Ergon. Soc. Annu. Meet.* **59**, 1027–1031 (2015).

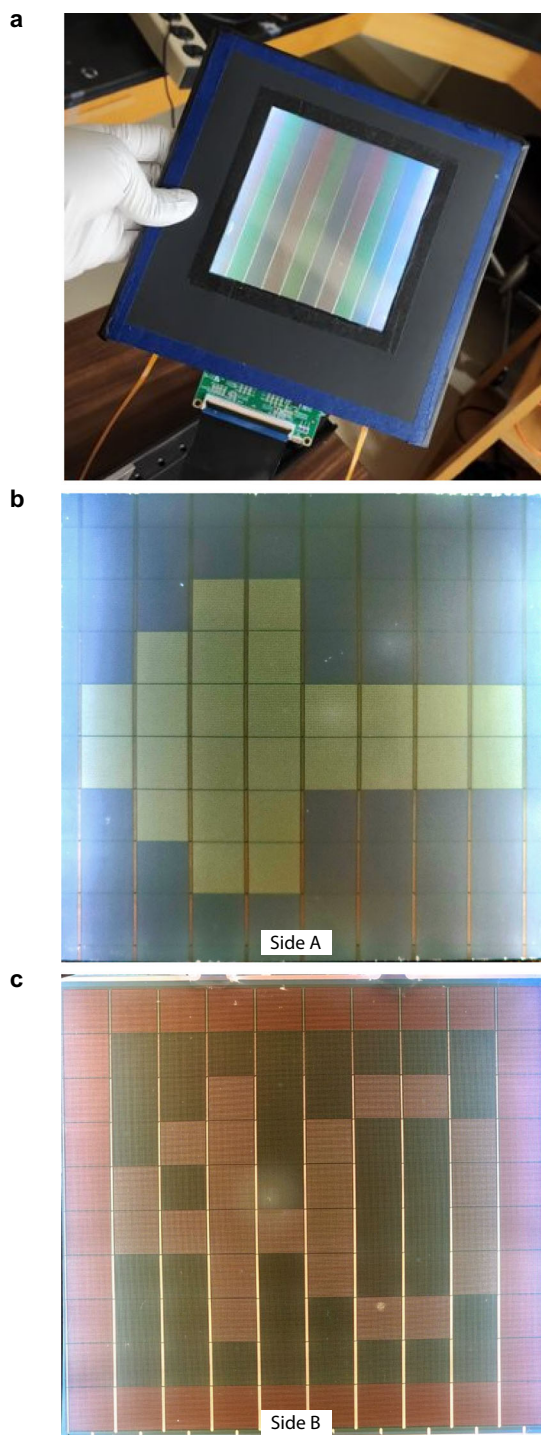


Fig. 5 | Prototype characteristics of the dual-sided, liquid crystal display.

a Image of the display in a housing while operating in ambient light conditions. The housing holds two sets of LEDs illuminating the waveguide display (not shown).

b The front side of the display shows an arrow pointing to the left. **c** Simultaneously the image on the backside of the display shows a street sign with the number 40 on it. The dark regions on the display correspond to transparent regions, however in order to capture the maximum brightness the images were taken in the dark.

Supplementary Movie 1 shows the dual-sided nature of the display and captures the corresponding transparency when the pixels are off in these locations.

5. Okumura, H. Human Centric AR & VR display and interface technologies for automobile. *IEEE Consum. Electron. Mag.* **8**, 60–61 (2019).
6. Jang, C., Bang, K., Chae, M., Lee, B. & Lanman, D. Waveguide holography for 3D augmented reality glasses. *Nat. Commun.* **15**, 66 (2024).
7. Lan, S. et al. Metasurfaces for near-eye augmented reality. *ACS Photonics* **6**, 864–870 (2019).
8. Lee, G.-Y. et al. Metasurface eyepiece for augmented reality. *Nat. Commun.* **9**, 4562 (2018).
9. Lee, S. et al. Tomographic near-eye displays. *Nat. Commun.* **10**, 2497 (2019).
10. Park, J. et al. Electrically driven mid-submicrometre pixelation of InGaN micro-light-emitting diode displays for augmented-reality glasses. *Nat. Photonics* **15**, 449–455 (2021).
11. Lindlbauer, D. et al. Tracs: transparency-control for see-through displays. In *Proc. 27th Annual ACM Symposium on User Interface Software and Technology*, (Association for Computing Machinery, New York, NY, USA 2014).
12. Jang, C. et al. Recent progress in see-through three-dimensional displays using holographic optical elements Invited. *Appl. Opt.* **55**, A71–A85 (2016).
13. Chen, J., Cranton, W. & Fihn, M. *Handbook of Visual Display Technology*. (Springer Publishing Company 2011).
14. L. G. Transparent OLED. <https://www.lg-informationdisplay.com/product/oled-signage/transparent-oled/55EW5PG-S> (2024).
15. OLED Space Transparent OLED. <https://www.oledspace.com/en/products/transparent-oled/#specifications> (2024).
16. Crystal Display Systems Transparent OLED Solutions. <https://crystal-display.com/products/transparent-cds-oled/> (2024).
17. Transparent OLED: TP-ZT110/ TP-ZT100 - Innovative Solution of Digital Display. <https://www.panasonic.com/my/consumer/audio-visual/televisions-learn/technology/transparent-oled-tp-zt110-tp-zt100.html> (2020).
18. Chen, H.-W., Lee, J.-H., Lin, B.-Y., Chen, S. & Wu, S.-T. Liquid crystal display and organic light-emitting diode display: present status and future perspectives. *Light Sci. Appl.* **7**, 17168 (2018).
19. Feng, Z., Wu, Y., Surigalatu, B., Zhang, X. & Chang, K. Large transparent display based on liquid crystal technology. *Appl. Opt.* **59**, 4915–4920 (2020).
20. Ungureanu, V.-I., Miclea, R.-C., Korodi, A. & Silea, I. A novel approach against sun glare to enhance driver safety. *Appl. Sci.* **10**, 3032 (2020).
21. JDI Transparent Display. <https://www.j-display.com/english/technology/jdinew/transparent-display.html> (2024).
22. Hainich, R. R. & Bimber, O. *Displays: Fundamentals and Applications*, (AK Peters, Wellesley, MA, USA, 2011).
23. Li, J., Greenberg, S., Sharlin, E. & Jorge, J. Interactive two-sided transparent displays: designing for collaboration. In *Proc. 2014 Conference on Designing Interactive Systems* (Association for Computing Machinery, New York, NY, USA, 2014).
24. Li, J., Greenberg, S. & Sharlin, E. A two-sided collaborative transparent display supporting workspace awareness. *Int. J. Hum. Comput. Stud.* **101**, 23–44 (2017).
25. De Guzman, J. A., Thilakarathna, K. & Seneviratne, A. Security and privacy approaches in mixed reality: a literature survey. *ACM Comput. Surv.* **52**, 1–37 (2019).
26. Lindlbauer, D., Lilija, K., Walter, R. & Müller, J. Influence of display transparency on background awareness and task performance. In *Proc. 2016 CHI Conference on Human Factors in Computing Systems* 1705–1716 (Association for Computing Machinery, New York, NY, USA, 2016).
27. Kohno, T., Kollin, J., Molnar, D. & Roesner, F. Display leakage and transparent wearable displays: investigation of risk, root causes, and defenses. <https://www.microsoft.com/en-us/research/publication/display-leakage-and-transparent-wearable-displays-investigation-of-risk-root-causes-and-defenses/> (2015).
28. Lindlbauer, D. et al. A collaborative see-through display supporting on-demand privacy. In *ACM SIGGRAPH 2014 Emerging Technologies* (Association for Computing Machinery, New York, NY, USA, 2014).
29. Allemeier, D. et al. Emergence and control of photonic band structure in stacked OLED microcavities. *Nat. Commun.* **12**, 6111 (2021).
30. Chen, R., Liang, N. & Zhai, T. Dual-color emissive OLED with orthogonal polarization modes. *Nat. Commun.* **15**, 1331 (2024).
31. Azuma, R. T. A survey of augmented reality. In *Presence Teleoperators and Virtual Environments*, **6**, 355–385 (MIT Press, Cambridge, MA, USA, 1997).
32. Zhu, J. & Pan, Z. Occlusion registration in video-based augmented reality. In *Proc. 7th ACM SIGGRAPH International Conference on Virtual-Reality Continuum and Its Applications in Industry* (Association for Computing Machinery, New York, NY, USA, 2008).
33. Moheghi, A., Qin, G. & Yang, D.-K. Stable polarizing light waveguide plate for edgelit liquid crystal displays. *Opt. Mater. Express* **6**, 429–435 (2016).
34. Moheghi, A., Nemati, H. & Yang, D.-K. Polarizing light waveguide plate from polymer stabilized liquid crystals. *Opt. Mater. Express* **5**, 1217–1223 (2015).
35. Zhou, X. et al. Full color waveguide liquid crystal display. *Opt. Lett.* **42**, 3706–3709 (2017).
36. Zhou, X., Qin, G., Dong, Y. & Yang, D.-K. Fast switching and high-contrast polymer-stabilized IPS liquid crystal display. *J. Soc. Inf. Disp.* **23**, 333–338 (2015).
37. Kreiml, P. et al. Balancing the electro-mechanical and interfacial performance of Mo-based alloy films. *Mater. Oxf.* **12**, 100774 (2020).
38. Han, L. et al. Wafer-scale organic-on-III-V monolithic heterogeneous integration for active-matrix micro-LED displays. *Nat. Commun.* **14**, 6985 (2023).

Acknowledgements

This study was supported by funding from MIRISE Technologies and Toyota Motor Corporation, Japan.

Author contributions

S.P.R., D.K.Y., & Y.G. designed and generated the device concept and execution plan. S.H., Y.S. prepared early-stage prototypes and performed experiments. S.H., Y.S., Y.P., L.W., L.D., G.Q., D.K.Y. designed and fabricated later-stage prototypes. S.H., Y.S., and S.P.R. characterized samples, documented, and generated data analytics and figures. S.H., S.P.R., D.K.Y., E.M.D., P.D.S., analyzed the data, and wrote and revised the manuscript.

Competing interests

The authors declare no competing interests.

Additional information

Supplementary information The online version contains supplementary material available at <https://doi.org/10.1038/s41467-024-54109-0>.

Correspondence and requests for materials should be addressed to Sean P. Rodrigues.

Peer review information *Nature Communications* thanks the anonymous reviewers for their contribution to the peer review of this work. A peer review file is available.

Reprints and permissions information is available at <http://www.nature.com/reprints>

Publisher's note Springer Nature remains neutral with regard to jurisdictional claims in published maps and institutional affiliations.

Open Access This article is licensed under a Creative Commons Attribution-NonCommercial-NoDerivatives 4.0 International License, which permits any non-commercial use, sharing, distribution and reproduction in any medium or format, as long as you give appropriate credit to the original author(s) and the source, provide a link to the Creative Commons licence, and indicate if you modified the licensed material. You do not have permission under this licence to share adapted material derived from this article or parts of it. The images or other third party material in this article are included in the article's Creative Commons licence, unless indicated otherwise in a credit line to the material. If material is not included in the article's Creative Commons licence and your intended use is not permitted by statutory regulation or exceeds the permitted use, you will need to obtain permission directly from the copyright holder. To view a copy of this licence, visit <http://creativecommons.org/licenses/by-nc-nd/4.0/>.

© The Author(s) 2024